Calculation of Solar Albedo and Radiation Equilibrium over the Qinghai–Xizang Plateau and Analysis of Their Climatic Features①

Zhao Ping (赵 平)② and Chen Longxun (陈隆勋)

Chinese Academy of Meteorological Sciences, Beijing 100081

(*Received October 20, 1998; revised September 20, 1999*)

ABSTRACT

Using radiation data from the Automatic Weather Stations (AWSs) for thermal balance observations, which were set up at Lhasa, Nagqu, Xigaze and Nyingchi by the Sino–Japanese Asian Monsoon Mechanism Co–operative Project in 1993–1996, and 1985–1989 Earth Radiation Balance Experiment (ERBE) measurements of Langley Research Center / NASA of US, and 1961–1996 monthly mean data from 148 surface stations over the Qinghai–Xizang Plateau (QXP) and its neighborhood, study is performed on empirical calculation methods of surface albedo, surface total radiation, planetary albedo and outgoing longwave radiation with the climatic features of radiation balance at the surface and the atmospheric top examined.

Evidences suggest that the empirical formulae for surface albedo, planetary albedo, surface total radiation and outgoing longwave radiation from the atmospheric top are capable of describing their seasonal and interannual variations over the QXP. The surface albedo is marked by noticeable seasonal variation and yearly mean of 0.22 with the maximum of 0.29 in January and minimum of 0.17 in July and August; in winter the albedo has great horizontal difference, bigger in the mountains than in the river valleys, and small in summer. The planetary albedo shows a smaller range of its annual variation with the yearly mean of 0.37, the maximum (minimum) occurring in February and March (autumn). In winter its high–value regions are mainly at Gar (Shiquanhe) in the western QXP and from the southwestern Qinghai to the northeastern Tibet and the low–value area at the northern slope of the central Himalayas; in summer, however, the albedo distribution displays clearly a progressive decrease from southeast to northwest. As for the surface total radiation, its values and annual varying range are smaller in the east than in the southwest. Its high–value center is at the southern slope of the Himalayas in winter and makes a conspicuous westward migration in spring, remaining there for a long time, and it begins to retreat eastward in autumn. Monthly mean values of the surface net radiation are all positive and larger in summer than in winter. The net radiation is significantly intensified under the combined effect of surface total radiation and surface albedo from spring to early summer, resulting in the strongest sector in the mid plateau with its center staying nearly motionless from March to September, and is reduced in autumn dominantly by surface effective radiation. The earth–atmosphere system loses heat outward from October to next February and gains in other months. On an average, the plateau gains heat of 15 W m^{-2} on an annual basis.

Key words: The Qinghai–Xizang Plateau, Albedo, Radiation balance, Climatic feature

①This work was supported under the auspices of the National (G1998040800) and CAS's Key Project for Basic Research on Tibetan Plateau (KZ951–A1–204; KZ95T–06).

②Present address: Department of Geophysics, Beijing University, Beijing 100871

1. Introduction

To precisely estimate the values of albedos at surface and atmospheric top, surface total radiation and earth–atmosphere outgoing longwave radiation is crucial to calculating radiation balance at surface and atmospheric top and exploring of the effect of the QXP atmospheric heat sources on atmospheric circulations.

Using 1958–1960 observations of surface total radiation, albedo and surface meteorological observations over China, Chen and Gong et al. (1964, 1965) investigated, through an atmospheric radiation calculation scheme, the distribution characteristics of planetary albedos all over China. They indicated that the albedos are small over the QXP in winter and summer, which leads to the fact that the greater part of solar radiation is absorbed by the earth–atmosphere system. Subsequently, Gao et al. (1977) and Xie (1984) made efforts to study the problem as well. By use of data from the 1979 QXPMEX Sun and Weng (1987) developed empirical expressions of surface albedo in relation to the number of snow-cover days and the temperature in the plateau and discussed the long-term mean of the albedo, showing that values of the albedo diminish conspicuously westward. From his study based on the QXP radiation observed from August 1982 to July 1983, Ji (1985) asserted that the surface albedo bears a relation to the class and intensity of precipitation and vegetation characteristics and that the albedo values are larger in summer than in winter. With the aid of the augmentation of satellite soundings, meteorologists made an approach to the relation ship between surface and planetary albedos in the QXP. Zhong et al. (1984, 1985, 1988) calculated planetary albedo by means of their model atmosphere over the plateau and soundings from AVHRR / NOAA, and established the regression formulae between planetary and surface albedos. Zhong (1998) recently investigated the features of surface albedo and the effect of snow cover on the albedo through the use of data from experiment of observing the QXP heat source from August 1982 to July 1983. Sun and Weng (1994) estimated the surface and planetary albedos in the QXP in terms of satellite data of ISCCP. Based on an earth–atmosphere physical model, Zhu and Zhu et al. (1993) derived the relation between surface and planetary abbedos under a clear sky. They further conducted experiments on the relation by using the measurements of surface radiation from the 1986 Sino–US QXP Co-Operative Research and the data from GAC of NOAA-9 in the same period. Weng (1994) proposed an empirical formula between planetary albedo and total cloudiness. By means of the radiation transfer method under a range of atmospheric and surface conditions, Li and Garand (1994) derived a parameterization scheme for surface albedo on a global basis from satellite soundings. Zuo et al. (1963), Weng (1964) and Lu et al. (1976) developed a fitting formula between surface total radiation and percentage of sunshine. Zhong et al. (1989) made an attempt to retrieve the QXP surface total radiation from satellite soundings. Weng (1997) reported their study on fitting the outgoing longwave radiation flux from the earth–atmosphere system by using surface or atmospheric temperature. The above studies have achieved many meaningful results. On the other hand, the complicated underlying surface of the plateau, paucity of measurements which came largely from a small number of stations set up during May–August of 1979 and August 1982–July 1983, and incompleteness of retrieval schemes from satellite data (e.g., no spectroscopic part of the measured surface albedo and simplicity of physical models) have led to the deviation of the gained surface albedo from its measurement in some parts of the plateau (see Zhu et al., 1993; Sun et al., 1994). As such, it is necessary to make further research of these problems in terms of an up-to-date dataset.

In terms of 1993–1996 AWS data, 1985–1989 ERBE observations at $2.5^{\circ} \times 2.5^{\circ}$

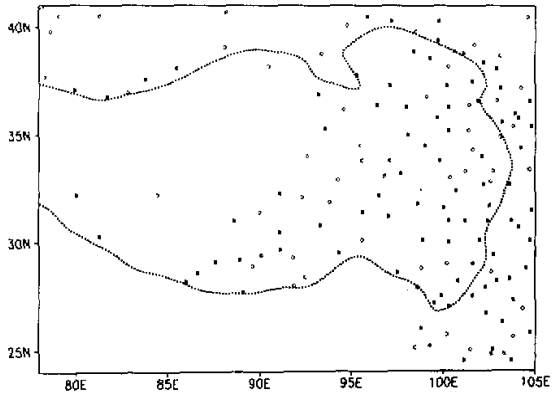

Fig. 1. The 148 stations over the QXP and its vicinity (The dotted line denotes the heights of 3000 m or more).

resolution of US Langley Research Center / NASA and 1984–1996 conventional measurements from the 148 stations over the QXP and its vicinity (Fig. 1), developed were the empirical expressions of surface albedo, surface total radiation, planetary albedo and outgoing longwave radiation that were then used to investigate the surface albedo and radiation balance at the surface and atmospheric top in the context of 1961–1995 monthly mean conventional data from the 148 stations, followed by the examination of their climatic features averaged over 1961–1990 that is known to be a WMO-defined period for the reference climatic means for the use in research.

2. Computational methodology

The expressions of radiation balance at the surface and atmospheric top are in the form, respectively

$$R_{\mathrm{net,s}} = S_{\downarrow}(1-A) - R_{\mathrm{e}}, \tag{1}$$

$$R_{\mathrm{net,t}} = S_{0\downarrow}(1-A_{\mathrm{p}}) - R_{\infty}, \tag{2}$$

where $R_{\mathrm{net,s}}$ represents the surface net radiation, $R_{\mathrm{net,t}}$ the net radiation at the atmospheric top, i.e., the earth–atmosphere net radiation, R_{e} the surface effective radiation (whose calculation and discussion are presented in Zhao and Chen (to be published in 2000)), A is the solar radiation reflected by surface, i.e., surface albedo, $S_{0\downarrow}$ the solar radiation arriving at the atmospheric top, A_p the solar radition reflected by the atmospheric top, i.e., planetary albedo, and R_{∞} the outgoing longwave radiation from the atmospheric top.

2.1 *The empirical formula of surface albedo*

The surface albedo A is defined as

$$A = \frac{S_{\uparrow}}{S_{\downarrow}}, \tag{3}$$

where $S_\uparrow$ denotes the surface-reflected solar radiation and $S_\downarrow$ the surface total radiation. Through (3) we calculate the surface albedo by use of AWS observations of $S_\uparrow$ and $S_\downarrow$ at different intervals from July of 1993 to July of 1996 (see Table 1). Here, the solar radiation wavelength ranges over 0.25–3 μ m. We took the data of radiation at a 10-minute interval, from which we obtained the daily and monthly means.

Table 1. Time intervals of the employed AWS data

	1993	1994	1995	1996	months
Lhasa	July–Dec.	Jan.–Dec.	Jan.–Dec.	Jan.–June	36
Nagqu	Oct.–Dec.	Jan.–Dec.	Jan.–Dec.	Jan.–June	33
Xigaze	July–Dec.	Jan.–July	July–Dec.	Jan.–July	26
Nyingchi	Aug.	Apr.–Nov.	July–Sept.	Jan.–June	18

Surface albedo refers to the ability of surface reflecting solar radiation and is in close association with the solar zenith angle and the surface condition, the latter bearing an intimate relation to climatic characteristics of a given region. The interannual and seasonal variations of local climate, differing from yearly growth of vegetation and soil condition, result from the integrative effects of meteorological elements, e.g., air temperature, pressure, vapor, wind, precipitation, cloud and snow cover. Therefore, the surface albedo is assumed to depend strongly on these elements. For instance, snow cover, if available, has conspicuous impacts on the albedo; in its absence, temperature, vapor, cloud and rainfall influence the surface albedo by affecting the growth and development of plants there. Analysis of the AWS surface albedo in relation to monthly means of surface weather elements indicates that the mean albedo is in correlation with mean temperature, relative humidity, pressure, total cloudiness, number of snow cover days and total rainfall on a monthly basis. As a result, we established a regression formula between the elements and the surface albedo on a monthly mean basis of July, 1993–July, 1996 for each of Lhasa (at 29.7°N, 91.1°E), Nagqu (at 31.5°N, 92°E), Xigaze (at 29.2°N, 88.9°E) and Nyingchi (at 29.6°N, 94.5°E) stations. The fitting formula for each has the following form:

for Lhasa, $$\hat{A} = (a_1 p + a_2) t_0^{a_3} e^{a_4 q} (r_a + a_5) c_1^{a_6} \quad , \tag{4}$$

for Nagqu, $$\hat{A} = (a_1 p + a_2)(t_0 + a_3) e^{a_4 q} r_a^{a_5} (c_1 + a_6) e^{a_7 (s_n + 1)} \quad , \tag{5}$$

for Xigaze, $$\hat{A} = (a_1 p + a_2)(t_0 + a_3) q^{a_4} (r_a + a_5)(c_1 + a_6) \quad , \tag{6}$$

for Nyingchi, $$\hat{A} = (a_1 p + a_2)(t_0 + a_3) e^{a_4 q + a_5 r_a} (c_1 + a_6)(s_n + a_7) \quad , \tag{7}$$

where $\hat{A}$ is the fitted value of A, t_0 the surface air temperature (K), $p = p_t / \overline{P}$ with p_t denoting monthly mean pressure and $\overline{P}$ the climatic mean of p_t, q the relative humidity (%), r_a the rainfall (mm), c_1 the total cloudiness in decimal form, $s_n (= n^* / n)$ the relative number of snow cover days with n^* signifying the total number of snow cover days in study months and n the number of days in a given month thereof, and $a_1, a_2, a_3, a_4, a_5, a_6$ and a_7 the regression coefficients (see Table 2 for their values). Moreover, to make Eqs.(4)–(7) meaningful, we set $r_a = 0.01$ or $c_1 = 0.01$ provided that $r_a = 0$ or $c_1 = 0$.

It is evident from Eqs.(4)–(7) that the discrepancy in form among the fitting expressions suggests so complicated topography of the plateau as to display vast difference in climatic features and surface condition and even in relative importance of the same element to the surface albedo for the different AWSs. We notice from Table 2 that the regression coefficients of

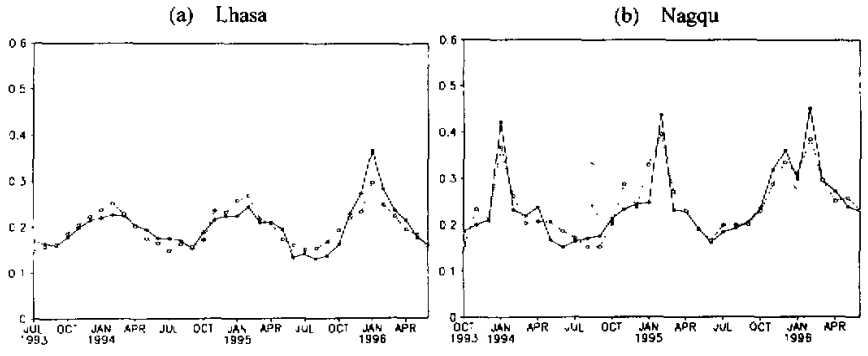

Fig. 2. The observed (solid line) and fitted (dotted) surface albedo on a monthly mean basis.

some of the elements involved differ in sign from station to station. Based on the correlation coefficients of these elements with the albedo, we discovered that for a single element, the sign of its correlation with the surface albedo is identical for all the AWSs except the magnitudes. The difference in the sign of the regression coefficients comes dominantly from the establishment of the multivariate regression equation. As we know, these meteorological factors are both inter–independent and inter–dependent. When one of the factors was introduced into the equation, possibly the role of the next was incorporated partially and has to be adjusted in order to get better fitting, thereby resulting in the fact that the regression coefficient of a given factor may differ in sign from one expression to another.

Fig. 2 presents the variation in monthly mean surface albedo observed and fitted at stations of Lhasa and Nagqu. One can see that the fitted curve describes the seasonal and interannual evolution in an approximate manner in comparison to the observations. To objectively verify the utility of the fitting formula for each of the AWSs, we calculated the statistic E of the time sequence X_i ($i=1, 2, \cdots, n$) of an element X, viz.,

$$E=\sqrt{\frac{1}{n}\sum_{i=1}^{n}\left(\frac{\hat{X}_i-X_i}{X_i}\right)^2}\ , \tag{8}$$

where $\hat{X}_i$ denoting the fitted X_i and E the averaged relative error of $\hat{X}_i$ from X_i. It follows from Eq.(8) that the smaller the E, the better would the fitting be. Table 3 gives the correlation coefficients r of the fitted surface albedo with the observed, and E for the four AWSs, from which we notice that all correlations are >0.8 and have passed test at $\alpha=0.01$ significance, with $r=0.88$ and 0.92 separately for Lhasa and Nagqu and $E=11.0\%$ and 6.0% for Nagqu and Nyingchi in turn. The mean r and E over the four AWSs reach 0.89 and 8.7%, respectively. As such, the correlation coefficients and the relative error (E) between the fitted and observed albedos meet the needs of climatic research such that we were allowed to use (4)–(7) to reveal the variation of the QXP surface albedo in a climatic context.

Table 2. Regression coefficients a_1 to a_7 for the four AWSs

	a_1	a_2	a_3	a_4	a_5	a_6	a_7
Lhasa	3.4×10^{15}	-3.8×10^{15}	−7.45	5.19×10^{-3}	−789.9	0.0734	
Nagqu	-5.4×10^{-4}	5.6×10^{-4}	−572.4	0.0113	−0.0574	−9.85	0.865
Xigaze	-4.4×10^{-6}	5.05×10^{-6}	−430.6	−0.3352	−1510.0	5.104	
Nyingchi	3.43×10^{-4}	-2.27×10^{-4}	−883.1	2.75×10^{-3}	-1.77×10^{-3}	−3.426	0.904

Table 3. Relation coefficients r and relative error E for the AWSs

Station	r	E (%)
Lhasa	0.88	10.6
Nagqu	0.92	11.0
Xigaze	0.83	7.2
Nyingchi	0.91	6.0

2.2 *The empirical formula of surface total radiation* $S_{\downarrow}$

Using the 1993–1996 AWS surface total radiation and the monthly total of sunshine hours we calculated the monthly mean surface total radiation and the percentage of sunshine. Subsequently, following Lu et al. (1976), we obtained an empirical expression for $S_{\downarrow}$ by virtue of the percentage of sunshine through a linear regression scheme. We have

$$\hat{S}_{\downarrow} = S_{0\downarrow}(a_1 t_{\odot} + a_2) , \tag{9}$$

where $t_{\odot}$ stands for the percentage of sunshine; a_1 and a_2 are the regression coefficients whose values are given in Table 4.

Table 4. Regression coefficients a_1 and a_2 for the AWSs

Station	Lhasa	Nagqu	Xigaze	Nyingchi
a_1	0.4259	0.5331	0.5005	0.6795
a_2	0.3703	0.3173	0.3265	0.2564

Fig. 3 delineates the variation of monthly mean observed and fitted $S_{\downarrow}$ for Lhasa and Nagqu, indicating that the fitted one describes well its seasonal and interannual variation. Further, the calculations show that the stations of Lhasa and Nagqu have the correlation of 0.88 and 0.85 and E of 4% and 5.4%, respectively. It is roughly the case at Xigaze and Nyingchi. Thus, the empirical expressions based on the percentage of sunshine for $S_{\downarrow}$ have ability to depict variation of the surface total radiation over the plateau in a climatic context. We can employ them as an approximate scheme for the surface total radiation in climatic research.

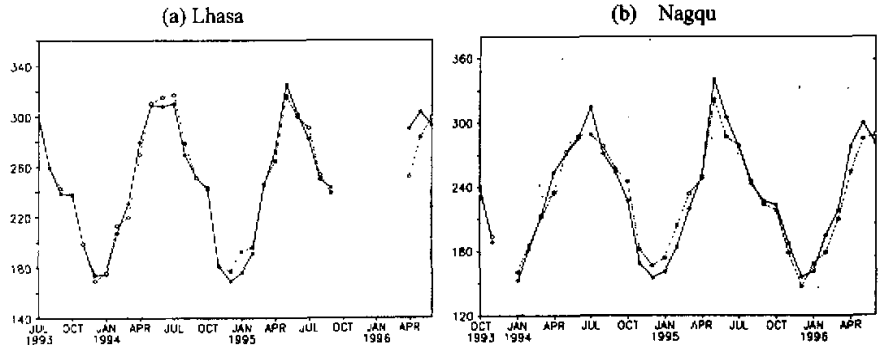

Fig. 3. The observed (solid line) and fitted (dotted line) values of surface total radiation (W m^{-2}) on a monthly mean basis.

Also, the fitting formulae of the surface total radiation for Chengdu (at 30.7°N, 104°E), Qamdo (at 31.1°N, 97.2°E) and Kunming (at 25.°N, 102.7°E) were used in dealing with S_1 for the QXP and its vicinity (Zhang et al., 1988). It is noted that the QXP involved was at a height of 3000 m or more, denoted by dotted line in Fig. 1, excluding those west of 90°E, north of 33°N.

2.3 *Empirical formulae of planetary Albedo (A_p) and earth–atmosphere outgoing longwave radiation R_∞*

Monthly mean A_p and R_∞ from the ERBE during January of 1985 and December of 1989 were interpolated into the 148 stations for corresponding A_p and R_∞, to which multivariate regression expressions were established with the aid of the monthly mean surface temperature, total cloudiness, relative humidity and the monthly total rainfall of these stations on a synchronous basis. Finally, we obtain the fitting formulae of A_p and R_∞, i.e.

$$\hat{A}_p = a_1 t_0 + a_2 c_1 + a_3 r_a + a_4 q + a_5 \ , \tag{10}$$

$$\hat{R}_\infty = b_1 t_0 + b_2 c_1 + b_3 r_a + b_4 q + b_5 \ , \tag{11}$$

where a_1 through a_5 and b_1 to b_5 are the regressions of A_p and R_∞, respectively, whose means are given in Table 5, where averaging was conducted over the QXP including the part east of 90°E and that west of 90°E, south of 33°N.

Table 5. Regression coefficients of a_1 to a_5 and b_1 to b_5 averaged over the plateau

Coefficients	a_1 / b_1	a_2 / b_2	a_3 / b_3	a_4 / b_4	a_5 / b_5
A_p	-3.8×10^{-3}	0.212	6.6×10^{-5}	-6.1×10^{-5}	1.27
R_∞	2.22	−60.9	-4.39×10^{-2}	0.229	−366.9

The horizontal distributions of correlation coefficients r of the fitted A_p and R_∞ with the observed ones and their respective relative error E (figure not shown) indicate that practically all the plateau A_p have the correlation larger than 0.80 with the minimum of the order of 0.70, and the QXP mean of 0.81; its values of E range over 5%–8% in most of the QXP, with the maximum of 8.6% at few stations and the QXP mean of 6.7%. The correlation coefficients of the fitted R_∞ with the observed are >0.90 except a limited number of regions in the south and the QXP mean attains 0.92; for R_∞, the values of E are $<4\%$ in most of the stations, with the maximum of 4.2% and the QXP mean of 2.7%. Fig. 4 portrays the distribution of 1985–1989 mean earth–atmosphere net radiation by dint of Eq.(2) as well as the fitted A_p and R_∞ versus the distribution of corresponding ERBE data in January and July. So we can see that the situation of the fitted values is similar to the observed in both January and July with the central regions well corresponding one to another. It follows that the empirical expressions for planetary albedo and atmospheric top outgoing longwave radiation, formulated with the aid of surface temperature, total cloudiness, precipitation and relative humidity, have considerable ability to describe their climatic features.

3. Climatic features of albedos in the QXP

3.1 *Surface albedo*

Using 1961–1990 conventional monthly mean data from the 148 stations and the fitting

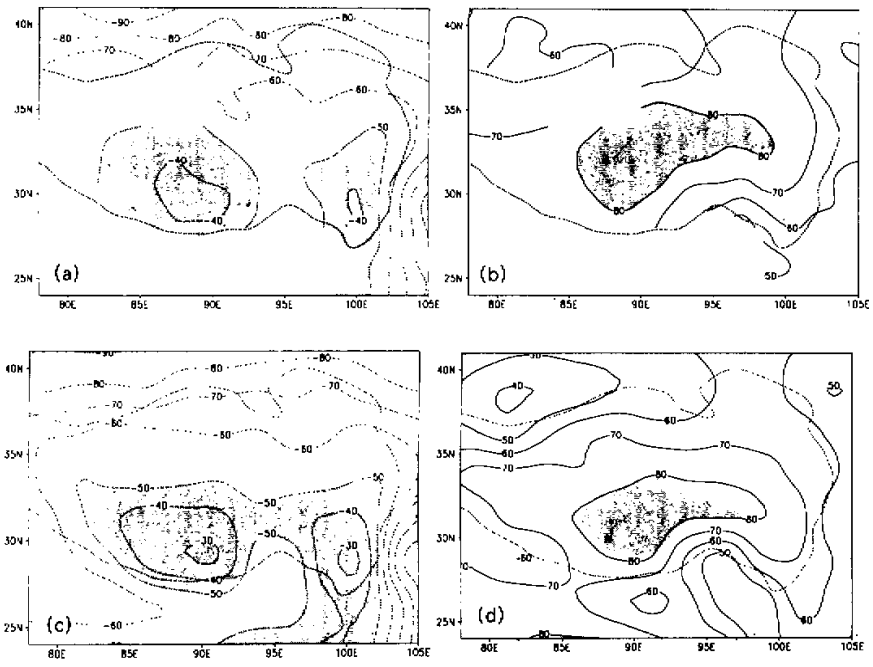

Fig. 4. 1985–1989 mean monthly earth–atmosphere net radiation flux (W m^{-2}). (a) January with the regions of fitted values >-50 W m^{-2} shaded; (b) July with the regions of fitted values >80 W m^{-2} shaded; (c) January with the regions of observed values >-50 W m^{-2} shaded; (d) July with the regions of observed values >80 W m^{-2} shaded.

expressions of surface albedo (4)–(7) for the four AWSs, calculation was performed of monthly mean albedos over the 30 years in such a way that for the AWSs (at Lhasa, Nagqu, Xigaze and Nyingchi) we adopted their own fitting formula and for the other stations took into account in choosing the fitting formula as follows: 1) the shortest distance in horizontal, 2) conditions of vegetation and soil, and 3) the Nyingchi expression used largely for the stations east of 95°E.

Table 6. 1961–1990 monthly mean surface albedos for the southwestern QXP, the eastern QXP and the QXP, and their annual means

Month	J	F	M	A	M	J	J	A	S	O	N	D	ANN.MEAN
SWQXP	0.29	0.28	0.25	0.21	0.20	0.18	0.17	0.17	0.18	0.19	0.21	0.25	0.22
EQXP	0.29	0.28	0.24	0.22	0.20	0.18	0.17	0.17	0.18	0.21	0.24	0.27	0.22
QXP	0.29	0.28	0.24	0.22	0.20	0.18	0.17	0.17	0.18	0.21	0.24	0.27	0.22

Table 6 gives the 1961–1990 monthly mean surface albedos for the two study segments. As stated earlier, the plateau involved was all at a height of 3000 m or more in the eastern part (east of 90°E) (EQXP) and in the southwestern part (west of the longitude, south of 33°N)

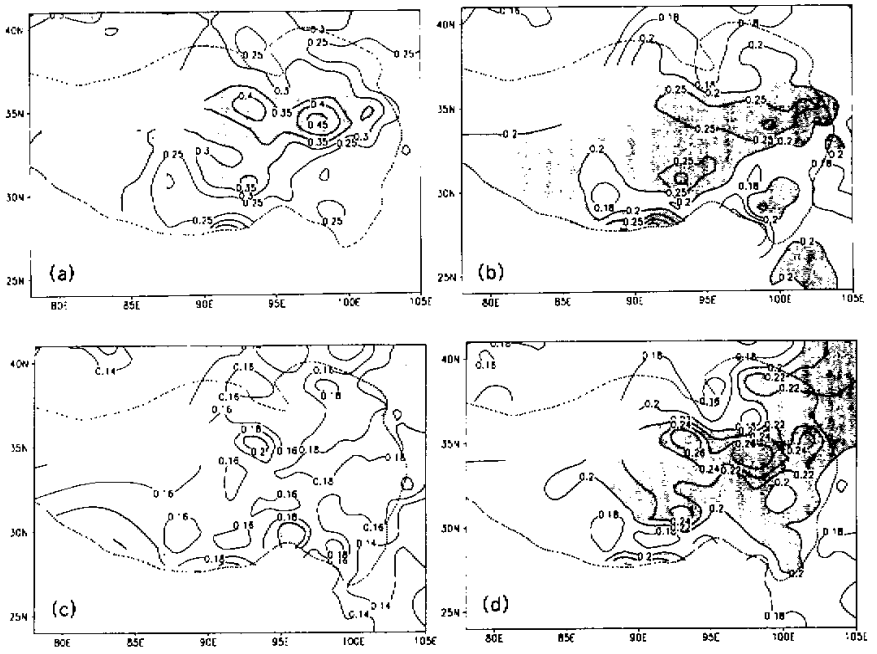

Fig. 5. 1961–1990 mean surface albedo on a monthly basis. (a) January with the regions of >0.3 shaded; (b) April with the regions of >0.2 shaded; (c) July with the regions of >0.18 shaded; (d) October with the regions of >0.2 shaded.

(SWQXP). The whole QXP refers to the sum of the two portions. The regional mean was obtained through the interpolation of data into $1° \times 1°$ gridpoints, followed by the addition and divided by the number of gridpoints. We notice from the table that the surface albedos in the two parts exhibit remarkable seasonal variation; it diminishes (increases) little by little from winter to summer (from summer to winter), maximizing at 0.29 in January and minimizing at 0.17 in July and August, and the regional means differ insignificantly.

Fig. 5 presents the distributions of QXP surface albedo on a monthly basis averaged over 1961–1990. In January (Fig. 5a) practically all the values are >0.20. The albedo differs greatly in the horizontal direction. Its high value sectors are dominantly in the mountains of the Tanggula, Bayan Har and Anyemaqen in the eastern QXP and the Himalayas and the Gangdise mountains in the southwestern QXP with the highest center of 0.46 situated around Madoi (at 34.9°N, 98.2°E) and Chindu (at 33.8°N, 97.1°E). The albedos are smaller over the Yarlung Zangbo River valleys, the southeast and northeast fringes of the plateau. In April (Fig. 5b) the pattern is similar to that in winter except remarkable reduction in magnitude. In July (Fig. 5c) the albedo keeps on decreasing and its horizontal difference is much smaller compared to the wintertime case, the values ranging over 0.16–0.18 for most of the plateau. This illustrates that in the wet season the vegetation develops well there, soil humidity increases, and the underlying surface approaches homogeneity such that the surface albedo and

its horizontal difference are reduced. In October (Fig. 5d) the albedo for the eastern plateau is greatly augmented with the high-value sector over the Bayan Har mountains and a low-value center in the Yarlung Zangbo River valleys.

3.2 *Planetary albedo*

The 1961–1990 monthly mean data of the 148 stations and the fitting formula (10) for planetary albedo were employed to investigate the features of the QXP planetary albedo averaged over this period.

The monthly means are summarized in Table 7 for three regions. One can see that the planetary albedo is conspicuously larger compared to the surface albedo, nearly twice as big as the surface albedo in summer, and that the planetary albedo has its annual range of 0.05 for either of the parts, much smaller than that of the surface albedo. Besides, the planetary albedo is slightly larger in the east than in the southwest and the yearly mean over the plateau reaches 0.37. It is large in February and March and small in October and November for either of the segments.

Table 7. 1961–1990 monthly mean planetary albedos in the southwestern QXP, the eastern QXP and the QXP, and their annual means

Month	J	F	M	A	M	J	J	A	S	O	N	D	ANN.MEAN
SWQXP	0.36	0.37	0.37	0.36	0.35	0.33	0.36	0.35	0.33	0.31	0.32	0.35	0.35
EQXP	0.38	0.40	0.40	0.39	0.38	0.38	0.37	0.36	0.37	0.35	0.35	0.36	0.37
QXP	0.37	0.39	0.39	0.39	0.37	0.36	0.37	0.36	0.36	0.34	0.34	0.36	0.37

Fig. 6 depicts the distribution of planetary albedo (A_p) on a monthly basis averaged over 1961–1990. In January (Fig. 6a) the high-value sectors are at Shiquanhe (at 32°N, 79°E) in the western QXP with its central value of 0.43 and from Tutu Heyan (at 34.2°N, 92.4°E) and Qumarleb (at 34.1°N, 95.8°E) in the southwestern Qinghai to Sog County (at 31.9°N, 93.8°E) in the northeastern Tibet with the center of 0.45; a low-value region resides at the northern slope of the mid-eastern Himalayas in the southern QXP and another is in the southeastern QXP. Inspection of Fig. 6a and the distribution of the number of snow-cover days and total cloudiness in January averaged over the same period (figure not given) show that the high- and low-value regions of planetary albedo well correspond to those of the latter two factors. As the warm season sets in, snow cover begins to melt, cloudiness grows, and the albedo increases slightly in value in the eastern and southern QXP as opposed to the slight reduction in the northern and southwestern QXP. In April (Fig. 6b) the high center that is in the eastern QXP in winter has moved southward to Zayu (at 28.7°N, 97.5°E) of the southeastern QXP; the high and low values are distributed in concord with the total cloudiness in most cases. Influenced by the total cloudiness in the wet season in July (Fig. 6c), A_p decreases gradually from southeast to northwest with its maximum value of 0.43 emerging in the southeast corner, significantly differing from those in Figs. 6a and 6b. It reduces to its annual minimum under the influence of diminishing cloudiness in October (Fig. 6d) when the rainy season has ended but no snow cover is available on ground and A_p values are larger in the eastern QXP than in the southwestern QXP.

The characteristics Figs. 6a and 6b show are different, to some degree, from the result of Chen, Gong and Wang et al. (1964) that a large-range low-value area of A_p is west of 100°E in January and July, centered around Lhasa. This arises from lack of data at that time.

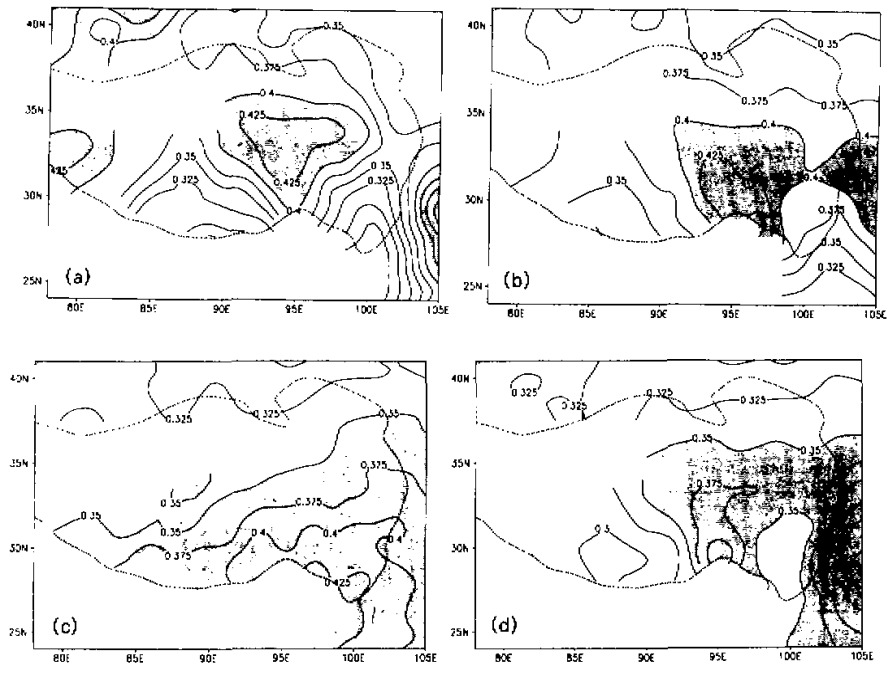

Fig. 6. 1961–1990 mean planetary albedo (%) on a monthly basis. (a) January with regions of >0.40 shaded; (b) April with regions of >0.40 shaded; (c) July with regions of >0.35 shaded; (d) October with regions of >0.35 shaded.

4. Climatic features of the QXP surface total radiation ($S_{\downarrow}$)

Table 8. 1961–1990 mean monthly surface total radiations (W m^{-2}) in the southwestern QXP, the eastern QXP and the QXP, and their annual means

Month	J	F	M	A	M	J	J	A	S	O	N	D	ANN.MEAN
SWQXP	180	209	259	304	335	340	307	291	276	248	204	174	261
EQXP	148	171	213	251	270	264	256	248	215	195	166	143	212
QXP	156	181	225	264	286	283	269	259	230	208	175	151	224

Values of surface total radiation ($S_{\downarrow}$) were calculated by use of (9) with the monthly means averaged over 1961–1990 and summarized in Table 8. We can see that $S_{\downarrow}$ is larger in the southwestern QXP than in the eastern QXP under the impacts of cloudiness. The southwestern QXP has its yearly range of 166 W m^{-2} in contrast to 127 W m^{-2} in the eastern QXP. The maximum $S_{\downarrow}$ occurs in May and June for both the portions and minimum in December and January. The mean maximum and minimum in the plateau reach 286 W m^{-2} and 151 W m^{-2}, respectively, annually averaging 224 W m^{-2}. $S_{\downarrow}$ grows most substantially in March in its course from spring to summer, with the monthly increment attaining

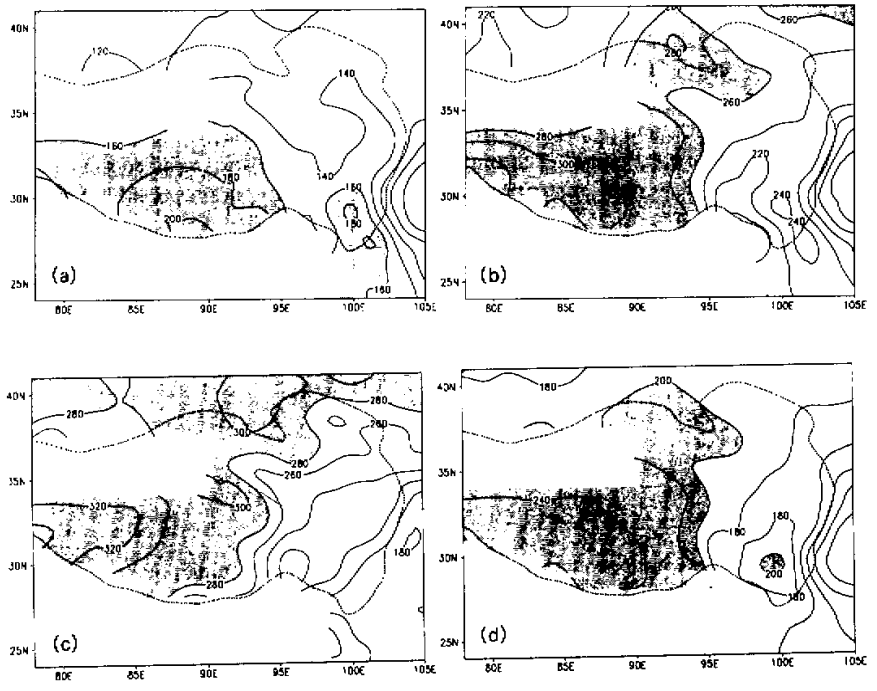

Fig. 7. 1961–1990 mean surface total radiation flux (W m^{-2}) on a monthly basis. (a) January with regions of > 160 W m^{-2} shaded; (b) April with regions of > 260 W m^{-2} shaded; (c) July with regions of > 280 W m^{-2} shaded; (d) October with regions of > 200 W m^{-2} shaded.

50 W m^{-2} and 42 W m^{-2} in the southwestern and eastern QXP, respectively, while from summer to winter it diminishes at a relatively slow pace.

Fig. 7 gives the distribution of the surface total radiation on a monthly basis averaged over the 30 years. In January (Fig. 7a) the high-value regions are located south of the Yarlung Zangbo River valleys and the Hengduan mountains of the southeastern plateau. Their strongest heating center is at Yadong (at 27.7°N, 89.1°E) on the southern slope of the Himalayas, staying there from December to March and peaking at 271 W m^{-2} in March and minimizing at the eastern fringe of the plateau. And later $S_{\downarrow}$ is greatly enhanced as spring comes. In April (Fig. 7b) the maximum heating center has moved westward to around Shiquanhe and Burang (at 30.5°E, 81.4°E) of the southwestern QXP from the Yarlung Zangbo River valleys and remains there during April–September, maximizing at 374 W m^{-2} as its annaul maximum in June. Also, Fig. 7b shows that a low sector covers Dege (at 31.7°N, 98.6°E) of the western Sichuan, Bomi (at 29.9°N, 95.8°E) and Zayu of the southeastern Tibet and the Gongshan (at 27.8°N, 98.7°E) of the northwestern Yunnan. In July (Fig. 7c) $S_{\downarrow}$ is reduced under the wet-season influence, and the heating center of the southwestern QXP has decreased to 342 W m^{-2}. Subsequently, the total radiation continues to diminish till October (Fig. 7d) during which the $S_{\downarrow}$ center of the southwestern QXP has retreated eastward into the Yarlung Zangbo River valleys (257 W m^{-2}). Comparison to the

result of Weng (1997) shows agreement in the pattern and central value during December and June.

5. Climatic features of surface and earth–atmosphere net radiation over the QXP

Substituting the monthly mean surface air temperature, relative humidity and total cloudiness, monthly total rainfall, sunshine hours and the fitted surface albedo into (1) and (2), we calculated the surface and earth–atmosphere net radiation on a monthly basis averaged over 1961–1990.

5.1 *Surface net radiation* $R_{net,s}$

Table 9. 1961–1990 monthly mean surface net radiations (W m^{-2}) in the southwestern QXP, the eastern QXP and the QXP, and their annual means

Month	J	F	M	A	M	J	J	A	S	O	N	D	ANN.MEAN
SWQXP	23	45	84	117	136	142	158	144	106	57	28	20	88
EQXP	19	43	83	112	128	137	134	121	96	58	25	13	81
QXP	20	44	83	113	130	138	140	127	99	58	26	15	83

From Table 9 we notice that the monthly means of surface net radiation are all positive. The magnitudes are somewhat larger in the southwestern QXP than in the eastern QXP, and their greatest difference arises in July and August (18% larger in the southwestern QXP). The maximum takes place in June and July for both the parts and the minimum in December and January. The means of the net radiation over the plateau are 140 W m^{-2} and 15 W m^{-2} in July and December, respectively, with the annual average 83 W m^{-2}. The net radiation grows during December–June, with minimum monthly increment of the order of 40 W m^{-2} in March, and begins to reduce from August, with the maximum monthly increment in October arriving at −41, −38 and −49 W m^{-2} for the QXP mean, the eastern and southwestern QXP, respectively. Inspection of Tables 6, 8 and 9, and the calculations of the surface effective radiation (Zhao et al., 2000) show that from spring to early summer, the surface net radiation grows due to increasing of the surface total radiation and decreasing of the surface albedo, and the persistent increase of the SW net radiation in July is mainly associated with weakening of the surface effective radiation there. When autumn starts, the variation in the surface effective radiation in particular, the surface total radiation and the surface albedo give rise to the reduction of the surface net radiation.

Fig. 8 presents the monthly patterns of the 1961–1990 mean surface net radiation. In January (Fig. 8a) the values are quite small in the plateau and even negative in parts of the eastern mountains, suggesting the heat loss from the surface. As spring comes, the surface net radiation begins to be reinforced, more strongly in the southwestern QXP than in the eastern QXP, which generates the strongest heating sector in the mid QXP to the south of the Tanggulas and north of the Himalayas. The heating area is maintained there from March to September with its center located dominantly at Amdo (at 32.5°N, 91.1°E) of the northeastern Tibet to Tutu Heyan of southwestern Qinghai from spring to mid–summer. The center peaks at 172 W m^{-2} as its yearly maximum in July (Fig. 8c). From August the center begins to move southeastward considerably with its value diminishing, and reaches Nyingchi of the eastern Tibet in October (Fig. 8d) with the central value of 101 W m^{-2}. Furthermore, we notice that in

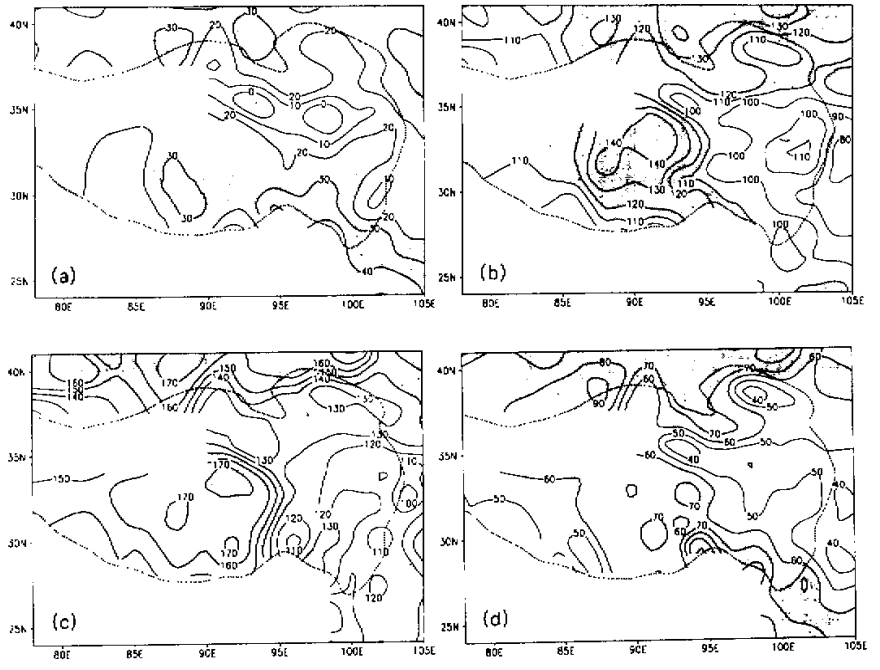

Fig. 8. 1961–1990 mean surface net radiation flux (W m^{-2}) on a monthly basis. (a) January with regions of >20 W m^{-2} shaded; (b) April with regions of >110 W m^{-2} shaded; (c) July with regions of >130 W m^{-2} shaded; (d) October with regions of >60 W m^{-2} shaded.

spring and summer the low–value regions are mainly in the mountains of the eastern Kunlun, Bayan Har and Qilian in the eastern QXP.

5.2 *Earth–atmosphere net radiation*

Table 10 shows the 1961–1990 monthly means of earth–atmosphere net radiation in the plateau. We notice that the monthly values are slightly larger in the southwestern QXP and increase (decrease) during January–June (July–December). In contrast to the surface net radiation, the earth–atmosphere counterpart has its negative values from October to February (suggestive of heat loss from the system). The earth–atmosphere net radiation has minima in December for the southwestern QXP, the eastern QXP and the QXP, with the value of −64 W m^{-2} as the QXP mean in December. It has positive values in March–September and the maximum in June, with the value of 83 W m^{-2} as the QXP mean in June. The earth–atmosphere system, on an average, gains heat of 15 W m^{-2} on an annual basis.

Table 10. 1961–1990 monthly means of earth–atmosphere net radiations (W m^{-2}) for the southwestern QXP, the eastern QXP and the QXP, and their annual means

Month	J	F	M	A	M	J	J	A	S	O	N	D	ANN.MEAN
SWQXP	−45	−13	26	60	83	90	79	61	33	−6	−42	−58	22
EQXP	−54	−23	14	49	73	80	73	52	19	−19	−52	−67	12
QXP	−52	−21	17	52	75	83	75	55	22	−16	−49	−64	15

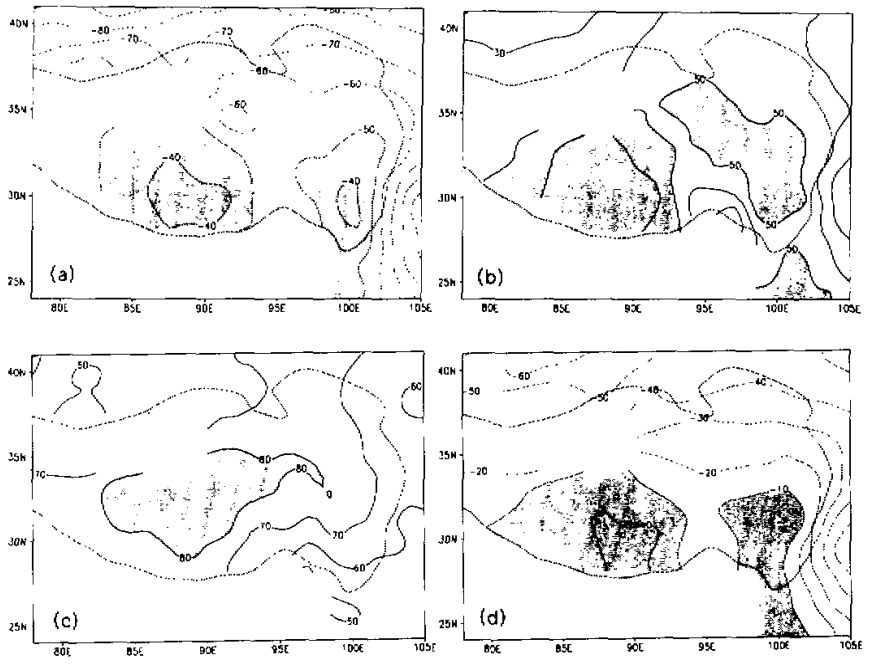

Fig. 9. 1961–1990 mean earth–atmosphere net radiation flux (W m^{-2}) on a monthly basis. (a) January with regions of >-50 W m^{-2} shaded; (b) April with regions of >50 W m^{-2} shaded; (c) July with regions of >80 W m^{-2} shaded; (d) October with regions of >-10 W m^{-2} shaded.

Fig. 9 illustrates the distributions of the earth–atmosphere net radiation on a monthly basis. In January (Fig. 9a) the values are <0 with maxima of -33 and -38 W m^{-2}, respectively at Nyemo (at 29.4°N, 90.2°E) of Tibet and Daocheng (at 29.1°N, 100.3°E) of Sichuan, which shows the situation typical of the winter half year. Referring to cloudiness data, the high sectors at Nyemo and Daocheng correspond to cloudless regions, suggesting that the small cloudiness is responsible for the augmentation of the absorption of solar radiation in the earth–atmosphere system. In spring the net radiation is enhanced conspicuously, particular in the southwestern QXP. Again, Fig. 9b indicates that the most intense center, although experiencing only small displacement in position in comparison to the wintertime case, is noticeably intensified and peaks at 94 W m^{-2} as the annual maximum in June. Moreover, another high sector emerges in April over the Baryan Har of the eastern QXP. In mid–summer (Fig. 9c) the earth–atmosphere net radiation is reduced to some extent because of considerably reinforced cloudiness and rainfall and its high center (87 W m^{-2}) has a short–distance eastward movement to Baingoin (at 31.4°N, 90°E) and Amdo of Tibet, followed by dramatic reduction. In October (Fig. d) the values of the net radiation have become negative practically all over the QXP.

6. Conclusions

In the context of the AWS measurements, the ERBE observations and the monthly mean data from the 148 stations, the empirical calculation schemes have been developed of surface albedo, surface total radiation, planetary albedo and outgoing longwave radiation. With the empirical formulae we first made the computation of monthly mean surface and atmospheric top albedos and radiation balance averaged over 1961–1990, alongside with their climatic features investigated. The following results are notable.

(1) The fitting expressions for surface and planetary albedos, surface total radiation and atmospheric-top outgoing longwave radiation are able to describe the seasonal and interannual variation of these factors over the QXP.

(2) The QXP surface albedo has its maximum of 0.27 (minimum of 0.17), on an average, in January (July–August). In wintertime months, it shows vast difference in horizontal, with its high-value regions dominating in the mountains of the eastern and southwestern QXP and its lower-value areas in the valleys of the Yarlung Zangbo River and the river valleys of the southeastern QXP. In summer the rainy season makes the underlying surface condition homogeneous, thereby reducing the horizontal difference.

(3) The yearly mean planetary albedo has the value of 0.37 for the QXP and small annual range of 0.05. The maximum of the albedo occurs in February–March, and the minimum in October–November. Influenced in winter by snow cover and total cloudiness, the albedo has its high-value regions at Shiquanhe and from Tutuhe and Qumarleb in the southwestern Qinghai to Sog in the northeastern Tibet. The low sectors are dominantly at the northern slope of the Himalayas in the southern QXP. As it becomes warm, the planetary albedo slightly grows in the eastern and southern QXP and diminishes in the southwestern and northern QXP. When the rainy season sets in, it exhibits a noticeable diminution from the southeastern QXP to the northwestern QXP. When the season has ended, cloudiness decreases there but no snow cover is present, thus leading to the reduction of the albedo to its annual minimum.

(4) Under the effect of cloudiness and rainfall, the surface total radiation ($S_{\downarrow}$) shows lower monthly mean and yearly range in the eastern QXP than in the southwestern QXP. In winter the maximum center is at the southern slope of the Himalayas where precipitation is scanty. As water vapor comes into the plateau from the eastern QXP in spring, the center of $S_{\downarrow}$ moves considerably westward and remains in the southwestern QXP till September. Afterwards, the center begins to withdraw eastward, accompanied by its noticeable reduction in the southwestern QXP.

(5) Surface net radiation values averaged in the QXP are positive on a monthly basis, maximizing (minimizing) at 140 (15) W m^{-2} in July (December). From spring to early summer, the net radiation is greatly enhanced under the joint action of surface total radiation and surface albedo, generating its strongest region in the mid plateau with its center almost motionless in March–September. In spring and summer, low-value regions of the net radiation are available mainly in the eastern mountains. In mid-summer, besides, its growth in the southwestern QXP is ascribed predominantly to the greatly reduced surface effective radiation, which contributes even more to the diminution of surface net radiation in autumn.

(6) The QXP earth-atmosphere system loses heat to outer space from October to next February and gains in the other months. It receives the heat of 15 W m^{-2}, on an average, each year. In spring the earth-atmosphere net radiation is enhanced to great extent, centering in the mid QXP and peaking in early summer.

REFERENCES

Chen Longxun, Gong Zhiben, Weng Yupu, and Sun Shouchun, 1964: Atmospheric radiation energy budget in East Asia (Part I). *Acta Meteor. Sinica*, **34(2)**, 146–161 (in Chinese).

Chen Longxun, Gong Zhiben, Chen Jiabin, and Ren Zejun, 1964: Atmospheric radiation energy budget in East Asia (Part II). *ibid.*, **34(3)**, 329–344.

Chen Longxun, Gong Zhiben, Chen Jiabin, and Wang Zhongxing, 1965: Atmospheric radiation energy budget in East Asia (Part III). *ibid.*, **35(1)**, 6–7.

Gao Guodong, and Lu Yurong, 1977: Study on Tibetan plateau radiation balance, thermal equilibrium and cold / heat sources, in *Collection of Papers for the Qinghai–Xizang Plateau Research* (1975–1976), edited and published by the Leading Group of Co–operative Study of Qinghai–Xizang Meteorology, 47–52, (internal issue, in Chinese).

Ji Guoliang, 1985: Radiation and climate in the Qinghai–Xizang Plateau for August, 1982–July, 1983. *Plateau Meteorology*, **4(4)**, 10–19 (Suppl. Issue, in Chinese).

Li Zhanqing, and L. Garand, 1994: Estimation of surface albedo from space: A parameterization for global application. *J. Geophs. Res.*, **99**, 8335–8350.

Lu Yurong, and Gao Guodong, 1976: Methods of calculating components of radiation balance and analysis of the space / time patterns over China (Part I). *J. Nanjing Univ.* (Edition of Natural Sciences), 89–110 (in Chinese).

Sun Zhi'an, and Weng Duming, 1987: Climatic calculation of surface albedo over China with its space / time distributions. *J. Nanjing Inst. Meteorology*, **10(2)**, 189–200 (in Chinese).

Sun Zhi'an, and Weng Duming, 1994: Qinghai–Xizang surface and planetary albedos. *J. Appl. Meteor.*, **5(4)**, 394–401 (in Chinese).

Weng Duming, 1964: Preliminary study of the scheme for climatic calculation of total radiation. *Acta Meteor. Sinica*, **34(3)**, 304–315 (in Chinese).

Weng Duming, 1994: Climatic features of planetary albedo over China, in Collected Papers on Congratulation to Professor Zhu Bianhai on the Sixtieth Anniversary of His Devotion to the Education and Research in the Meteorological Context (Spec. Issue). *J. Nanjing University*, 80–87 (in Chinese).

Weng Duming, 1997: *Radiation Climate in China*, China Meteorological Press, Beijing, 129–132 and 318–324 (in Chinese).

Xie Xianquan, 1984: Qinghai–Xizang surface albedo in May–August, 1979, in *QXPMEX Symposium (II)*, Science Press, Beijing, 17–23 (in Chinese).

Zhang Jijia, Zhu Baozhen et al. 1988: *Advances in Qinghai–Xizang Meteorology*, Science Press, Beijing, 35–38 (in Chinese).

Zhao Ping and Chen Longxun, 2000: Study on climatic features of surface turbulent heat exchange coefficients and surface thermal sources over the Qinghai–Xizang Plateau. *Acta Meteor. Sinica* (to be published).

Zhong Qiang, 1984: AVHHR data calculated planetary albedo and outgoing longwave radiation in the Qinghai–Xizang Plateau, *Plateau Meteorology*, **3(2)**, 1–9 (in Chinese).

Zhong Qiang, 1998: Characteristics of variation in surface albedo and snow forcing over the Tibetan Plateau. *Acta Meteor. Sinica*, **12**, 177–189.

Zhong Qiang, and Qi Jin'e, 1989: Estimation of Qinghai–Xizang total radiation by use of Nimbus–7 planetary albedo observations. *Acta Meteor. Sinica*, **42(2)**, 165–172 (in Chinese).

Zhong Qiang, and Wu Shijie, 1985: On the Methods of AVHHR data–derived Qinghai–Xizang surface albedo. *Plateau Meteorology*, **4(3)**, 193–203 (in Chinese).

Zhong Qiang et al., 1988: Satellite observation of surface albedo over the Qinghai–Xizang Plateau region. *Advances in Atmospheric Sciences*, **5(1)**, 57–85.

Zhu Changhan, Zhu Fukang, and Liu Yujie, 1993: Research on Qinghai–Xizang clear–sky planetary albedo in relation to surface albedo. *Acta Meteorologica Sinica*, **51(1)**, 57–65 (in Chinese).

Zuo Dakang et al., 1963: Spatial distribution features of solar total radiation over China. *Acta Meteor. Sinica*, **33(1)**, 409–415 (in Chinese).